

Unsteady aerodynamic modeling based on fuzzy scalar radial basis function neural networks

Proc IMechE Part G:
J Aerospace Engineering
2019, Vol. 233(14) 5107–5121
© IMechE 2019
Article reuse guidelines:
sagepub.com/journals-permissions
DOI: 10.1177/0954410019836906
journals.sagepub.com/home/pig



Xu Wang^{1,2}, Jiaqing Kou^{1,2} and Weiwei Zhang^{1,2}

Abstract

In this paper, a fuzzy scalar radial basis function neural network is proposed, in order to overcome the limitation of traditional aerodynamic reduced-order models having difficulty in adapting to input variables with different orders of magnitude. This network is a combination of fuzzy rules and standard radial basis function neural network, and all the basis functions are defined as scalar basis functions. The use of scalar basis function will increase the flexibility of the model, thus enhancing the generalization capability on complex dynamic behaviors. Particle swarm optimization algorithm is used to find the optimal width of the scalar basis function. The constructed reduced-order models are used to model the unsteady aerodynamics of an airfoil in transonic flow. Results indicate that the proposed reduced-order models can capture the dynamic characteristics of lift coefficients at different reduced frequencies and amplitudes very accurately. Compared with the conventional reduced-order model based on recursive radial basis function neural network, the fuzzy scalar radial basis function neural network shows better generalization capability for different test cases with multiple normalization methods.

Keywords

Neural network, fuzzy radial basis function, reduced-order model, system identification, unsteady aerodynamics

Date received: 31 August 2018; accepted: 14 February 2019

Introduction

In the past decades, artificial neural networks (ANNs) have been successfully employed in many applications such as system identification and control^{1–3} and time series prediction.^{4–6} Considering the advantages of the recursive neural networks (RNNs) and the radial basis function (RBF) performed in the previous research, the researchers began to use the RNNs⁷ and the recursive radial basis function (RRBF) neural network,^{8,9} in order to realize the prediction of nonlinear aerodynamics. This paper proposes a method to enhance the generalization capability of the aerodynamic models based on the neural network.

With complex nonlinear and unsteady effects, aerodynamic systems are complicated with strong time-delay effects compared to conventional dynamic systems.¹⁰ Although computational fluid dynamics (CFD) method is widely used in fluid mechanics, the large computational cost makes it inappropriate for aeroelastic analysis, design optimization, or other applications. Therefore, in recent years, researchers have successfully developed a variety of aerodynamic reduced-order models (ROMs) based on the CFD method. These models have high precision and

simple structure, which can replace the CFD to realize unsteady flow field calculation and shorten the calculation time by one and two orders of magnitude.¹¹ ROM has been widely applied in flight dynamics, fluid-structure interaction, flow control, and optimization design.^{12–15}

Currently, unsteady aerodynamic ROMs can be divided into two categories: the proper orthogonal decomposition (POD)^{16,17} or the system identification. POD-based ROMs require the high-dimensional snapshots to reduce the dimensionality of the governing equation. However, the system identification method only needs the input and output samples from CFD and constructs an input–output relationship from a black-box perspective. These methods mainly include linear autoregressive with exogenous (ARX)

¹School of Aeronautics, Northwestern Polytechnical University, Xi'an, China

²National Key Laboratory of Aerodynamic Design and Research, Northwestern Polytechnical University, Xi'an, China

Corresponding author:

Jiaqing Kou, School of Aeronautics, Northwestern Polytechnical University, Xi'an 710072, China.

Email: koujiaqing93@163.com

models,^{18,19} eigensystem realization algorithm (ERA),^{20,21} Volterra series,^{22–24} indicial function models,^{25,26} Kriging model,^{27–29} neural network,^{9,30} Wiener models,^{31,32} and so on.

The neural network model has the characteristics of self-learning, self-adaptive, and fault-tolerance. It is also able to approximate any function at arbitrary precision. Due to such advantages of the neural network, it is rapidly applied to unsteady aerodynamic modeling problems. Kurtulus⁷ used ANN to model the unsteady aerodynamic force coefficients of flapping motion kinematics. The RRBf neural network developed by Zhang et al.⁹ introduced output feedback for the standard RBF neural network to reflect the unsteady dynamic effects. With the RRBf reduced-order model, they predicted the aeroelastic limit cycle oscillation response in transonic flow. However, in this work, the model parameters are mainly determined by the inconvenient trial-and-error method, and the training signals are carefully designed with a small frequency range, which limited the model's generalization capability. Besides, Ghoreyshi et al.³³ used RBF models, Mannarino and Mantegazza⁸ used recurrent neural networks to model the unsteady aerodynamics and applied this model to aeroelastic problems, and Winter³⁴ used the neurofuzzy model to predict the unsteady aerodynamic loads and the flutter boundary. Dey et al.³⁵ introduced Reynolds numbers, Prandtl numbers, and various corner radii as input parameters to predict the unsteady forced convection.

To improve the generalization capability of existing models, there are mainly two groups of ideas: (1) Developing effective training algorithms with a fixed model framework. Kou and Zhang³⁶ introduced a width optimization method with a validation case, optimized the width of each neuron in the hidden layer, and obtained a multiscale RBF neural network dynamic model.³⁷ This method avoids the model from failing into overfitting and makes the model take into account the training and prediction performance; Mannarino and Mantegazza⁸ used standard and automatic differentiation integration techniques in the training of network synaptic weights, and compared the differences of their generalization capabilities. Zhang et al.³⁸ proposed an effective center selection algorithm based on the proper orthogonal decomposition (POD), which extracts features in samples before model training. These methods all enhanced the model's generalization capability without changing the model structure. (2) Changing the model framework to increase its degree of freedom. This idea introduces additional parameters to the model and give it better adaptation on complicated dynamic behaviors. For example, Fernández-Navarro³⁹ proposed the generalized radial basis function (GRBF) neural network. Through optimizing the parameter τ of the generalized Gaussian distribution, the active functions of the network are more flexible to enhance the generalization capability. Kou and Zhang⁴⁰ proposed a multikernel

neural network, which combines Gaussian basis function with wavelet basis function in the hidden layer to allow the model to approximate multiple types of nonlinear features. Winter and Breitsamter⁴¹ proposed a multilayer neural network, which is combined with recurrent linear neuro-fuzzy model to lead to an enhanced simulation and generalization performance. Besides, Han and Qiao⁴² proposed a recurrent self-organizing neural network (RSOINN), with the adaptive growing and pruning algorithm, the hidden neurons of RSOINN can be added or pruned improve the generalization performance.

Since most of ROMs are multi-input and multioutput models, the differences between the input magnitude should be considered during the training process. For example, the lift and moment coefficients, C_l and C_m , are usually at two different magnitudes. Therefore, we always use the normalization method to overcome the difficulties in training such a multi-input neural network model. But this method is empirical and has no universal guidelines. Besides, when the data of the signal are changing greatly with time, the normalization may not guarantee a good performance. Such multi-scale problems cannot be solved by the traditional method, which combines the shallow neural network model and a normalization process. The other way for this problem is to establish a deep neural network model. However, the training and optimization process for deep neural networks are complicated, and the resulting model structure is complex as well. Therefore, a new structure of the neural network model is preferred, which is not only adaptive to different input types but also has a relatively simple structure.

In the current study, both methods mentioned before to improve the generalization capability are used to obtain a better aerodynamic ROM. The particle swarm optimization (PSO) algorithm is used to determine the unknown parameters. The model framework of standard RBF network is improved by adding fuzzy rules and utilizing scalar basis functions. The introduction of fuzzy rules, will help to construct a four-layer neural network with a more flexible model structure. For standard RBF neural networks, when the vector basis function is directly used, each value of the system input is coupled, and the physical and scale differences between different inputs may be ignored. Therefore, a scalar basis function modeling approach is introduced to accommodate the differences between the different scales and different input types. Through the optimization of the width, the scalar basis function can reflect the feature differences between the input parameters from different widths. In the following test cases, this new model shows higher accuracy and better generalization capability, especially in modeling input parameters at different scales.

The present paper is organized as follows. The upcoming section describes the differences between

the FSRBF neural network and the traditional RRBF neural network. Introduction of the CFD numerical method is shown next. The reduced-order modeling methodology is tested in a later section, where complex aerodynamic problems of lift coefficients in transonic, viscous flows are studied. Last section concludes the current study.

Neural network model

Recursive RBF neural network

The essence of unsteady aerodynamics is the time-delayed effects, which can be represented by the following dynamic model with input delay and output feedback

$$\begin{aligned} y(k) &= f[x^T(k)] \\ &= f\{[u^T(k), u^T(k-1), u^T(k-2), \dots, u^T(k-m), \\ &\quad y^T(k-1), y^T(k-2), \dots, y^T(k-n)]\} \end{aligned} \quad (1)$$

where u , x , y are the input, state, and output vectors, respectively. k is the current time step. This model is a typical nonlinear autoregressive with exogenous input (NARX) model.⁴³ Based on this framework, Zhang et al.⁹ extended the static RBF neural network to a RRBF neural network. Li et al.²⁸ combined the Kriging function and recurrence framework together and proposed a new framework of ROM to solve the unsteady aerodynamics problem of NACA0012 airfoil. The RRBF neural network model is a typical three-layer neural network consisting of input layer, hidden layer, and output layer. In the prediction phase, the input vector is transformed by a nonlinear mapping through the radial basis function of the hidden layer and is then linearly superimposed on the output layer to obtain the current system output. The model workflow is shown in Figure 1. In the current study, this model is used as a benchmark aerodynamic ROM for comparison purpose.

FSRBF neural network

The fuzzy inference system and the RBF network are functional equivalent under some minor restrictions. This functional equivalence implies that advances in each literature, such as new learning rules or analysis on representational power, etc., can be applied to both models directly.⁴⁴ As a result, Boely et al.⁴⁵ have used the fuzzy logic and neural network to identify the nonlinear F/A-18 model in 2011. Using the fuzzy logic, the standard RBF neural network can be transformed into FRBF neural networks⁴⁶ with a higher degree of freedom. The model workflow is shown in Figure 2. The fuzzy scalar radial basis function (FSRBF) neural network developed in this paper is a four-layer network, including input layer, fuzzy

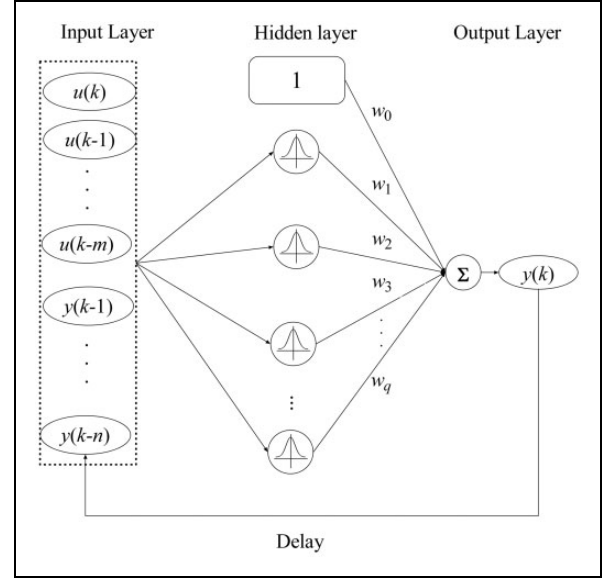


Figure 1. Recursive RBF neural network.

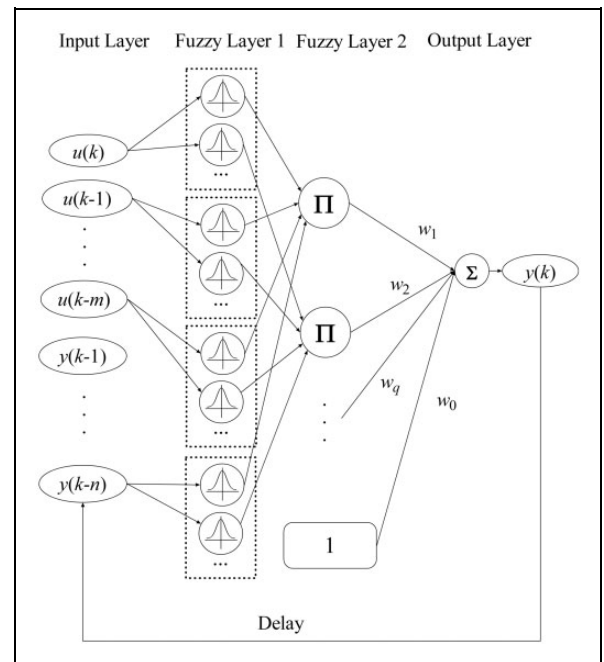


Figure 2. FSRBF neural network.

layer 1, fuzzy layer 2, and output layer. Such model has a similar structure with the recurrent RBFN-based self-learning fuzzy-neural-network (RRSEFNN) designed for the control of fuzzy system,⁴⁷ but in order to solve a different problem, i.e. nonlinear aerodynamic identification, more complicated training processes with PSO algorithm are used.

In the input layer, each entry of the state vector is used as the input parameters separately. Different from the RRBF neural network, the input layer in FSRBF neural network is represented by scalar parameters. In equation (2), in the fuzzy layer 1, the input scalar is then mapped through a basis function to

achieve a nonlinear transformation. The center of each hidden layer c_{ij} is selected from the training case. Through adjusting the width σ_{ij} in the scalar basis function g , the influence of each input parameter is easily reflected, thereby decoupling the input vector. The selection of basis function will be discussed in Section 2.3.

$$f_2(i, j) = g(f_1(i), c_{ij}, \sigma_{ij}) \quad (2)$$

In fuzzy layer 2, the scalars in fuzzy layer 1 are multiplied to achieve the fuzzification. Here, N denotes the time memory effect caused by unsteady effects, which is the sum of input and output delay orders. The input of the relevant time series has a coupling effect on the current system output. The “product summation” process is widely used in fuzzy system. It reduces the number of neurons in fuzzy layer 2 and well reflects the aerodynamic hysteresis effect.

$$f_3(j) = \prod_{i=1}^N f_2(i, j) \quad (3)$$

In the output layer, each f_3 will be linearly superimposed to get the system output. w_j is the weight that connects fuzzy layer 2 neuron number j to the output neuron $y(k)$

$$y(k) = w_0 + \sum_{j=1}^c w_j \cdot f_3(j) \quad (4)$$

Therefore, the fuzzy RBF neural network is expressed as

$$y(k) = w_0 + \sum_{j=1}^c w_j \cdot \prod_{i=1}^N g(f_1(i), c_{ij}, \sigma_{ij}) \quad (5)$$

Scalar radial basis function

Currently, there are many types of basis function for RBF neural network. Gaussian RBF, multiquadric RBF, inverse multiquadric RBF, thin-plate spline RBF, and wavelet RBF have been proposed in previous studies. Here, two basis functions, the Gaussian basis function and inverse multi-quadratic basis function, are used for the comparison purpose.

$$g(r^2) = \exp\left(-\frac{r^2}{2\sigma^2}\right) \quad (6)$$

In equation (6), Gaussian function is expressed as function g . r is the difference between the neuron input x and the neural center c , which is expressed as $|x - c|$. The basis function provides the nonlinear mapping to the input. The width indicates the range

of influence of the neurons. The larger the width, the greater the range of influence of the neurons and the smoother the curve, and vice versa.

$$g(r^2) = \frac{1}{\sqrt{\sigma^2 + r^2}} \quad (7)$$

The inverse multiquadratic basis function shown in equation (7) is also used. The effect of the width is opposite to that of the Gaussian function. A larger width will lead to a smaller output and a smaller influence range. Based on the above two basis functions, two neural network models with either Gaussian or inverse multiquadratic basis functions as the activation function are constructed and compared in the following study.

Optimization algorithm

The PSO algorithm was proposed by Kennedy and Eberhart⁴⁸ in 1995. This method regards the parameters to be optimized as particles, calculate the fitness through the partial movement, and iteratively obtains the global optimal solution.

$$\begin{aligned} V_i^{d+1} = & \omega(t) \times V_i^d + c_1 r_1 \times (P_i^d - X_i^d) + c_2 r_2 \\ & \times (Gbest_i^d - X_i^d) \end{aligned} \quad (8)$$

$$X_i^{d+1} = X_i^d + V_i^{d+1} \quad (9)$$

$$\omega(t) = \omega_2 - (\omega_2 - \omega_1) \times d/G \quad (10)$$

In PSO algorithm, $X = [X_1, X_2, \dots, X_{Size}]$ represent the parameters to be optimized (the location of the particle). Equation (8) shows the change in the particle update rate, d is the current number of iterations. The local fitness $P = [P_1, P_2, \dots, P_{Size}]$ and the global optimal fitness $Gbest$ of each particle are reflected in equation (8). Inertia weights are updated through equation (10), ω_1 and ω_2 are the lower and the upper bounds of the weights, and G represents the number of iterations. r_1 and r_2 are the mutation probabilities in the process of particle evolution, and learning factors c_1 and c_2 control the speed of particle learning. By updating the particle position through equation (9) until the iteration stops, the global optimal solution can be obtained. Kou and Zhang³⁶ developed a method of aerodynamics modeling with validation cases in combination with the PSO algorithm and enhance generalization capability of the aerodynamic ROM. In the present study, this optimization algorithm is also used to determine the unknown widths of the scalar basis functions.

The model is trained as follows: firstly, a set of width is given by the PSO algorithm, and the center is selected from the input samples. Secondly, all the input training samples are mapped by the basis function, and the

matrix for the fuzzy layer output is calculated. At last, the weights are calculated by the least-squares method, and the model is finally obtained.

CFD solver

To establish the aerodynamic ROM, the training case is needed. This case is calculated from the full-order CFD solver, which solves the aerodynamic loads from the forced airfoil motion. The CFD solver is based on the unsteady Reynolds-averaged Navier–Stokes (URANS) equations. The integral form of this equation is given as follows

$$\frac{\partial}{\partial t} \iiint_{\Omega} W d\Omega + \iint_{\partial\Omega} F(W) \cdot \mathbf{n} dS = \iint_{\partial\Omega} F_v \mathbf{n} dS \quad (11)$$

where $W = [\rho, \rho u, \rho v, \rho e]^T$ denotes the conservation vector, and Ω is the control volume. \mathbf{n} represents the outer unit normal vector to the boundary $\partial\Omega$. In conservation vector, ρ represents the density of the fluid, u is the x -axis velocity, v is the y -axis velocity, and e represents the total internal energy per unit mass of fluid. $F(W)$ is the amount of circulation and F_v represents the viscous flux. The nondimensional time step DT is set to 0.4, in order to capture a large range of frequency. The flow conditions are Mach number $Ma = 0.8$ and the Reynolds number is designed as 3,000,000.

To accurately capture the viscous aerodynamic effects in transonic flow, we select the Spalart–Allmaras (S–A) turbulence model⁴⁹ to enclose the governing equations and describe the turbulence fluctuations. The CFD solver allows moving bodies through using an arbitrary Lagrangian–Eulerian formulation and the dynamically deforming mesh algorithm is based on RBF interpolation.⁵⁰ To accelerate the convergence of time-marching, local-time stepping, residual smoothing, and multigrid are all equipped. The hybrid computational mesh of the NACA0012 airfoil

with 6004 nodes (180 surface nodes) and 8568 cells is used to verify the accuracy of the CFD solver. The y^+ number is less than 1.3 in most of the regions and the distance between the airfoil and the circular far field is $20c$. Figure 3 shows the computational mesh of the NACA0012 airfoil in detail. Further details of the CFD solver can be found in [51,52].

The accuracy of the flow solver has been validated in [12], [13] and [15], where the CFD results are compared with experimental or numerical simulation results. To verify the accuracy of the CFD solver, the results of lift and moment coefficients are compared with experimental results of AGARD CT Case 5.⁵³ The comparison results in Figure 4 show that the CFD solver agrees well with the experimental data.

Result and discussion

In order to demonstrate the capability of the proposed model in modeling unsteady aerodynamics, the NACA0012 airfoil pitching in the transonic flow at Mach number 0.8 is chosen as the test case. The steady flow of NACA0012 airfoil at 0° angle of attack (AOA) is shown in Figure 5. The Reynolds number is designed as 3,000,000.

The airfoil's lift coefficient of pitching motion around the 25% chord length is identified. The pitching angle is used as the input case, and the lift coefficient calculated by the CFD (N–S equations) is used as the output for training. To evaluate the generalization capability, the test cases at different amplitudes and frequencies, with both linear and nonlinear aerodynamics, are considered. The nondimensional step size of the signal is calculated by the following equation

$$DT = dt / (2 * b / a) \quad (12)$$

where dt is the physical time step, b is the half chord length, and a is the velocity of the sound in free-stream. In this study, DT is set to 0.4, in order to allow a sufficient coverage of frequency content.

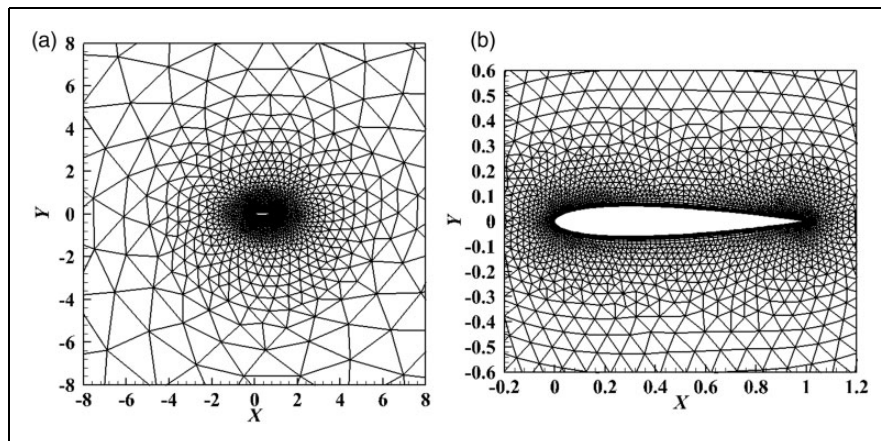


Figure 3. Computational mesh (NACA0012 airfoil): (a) global view; (b) close-up view.

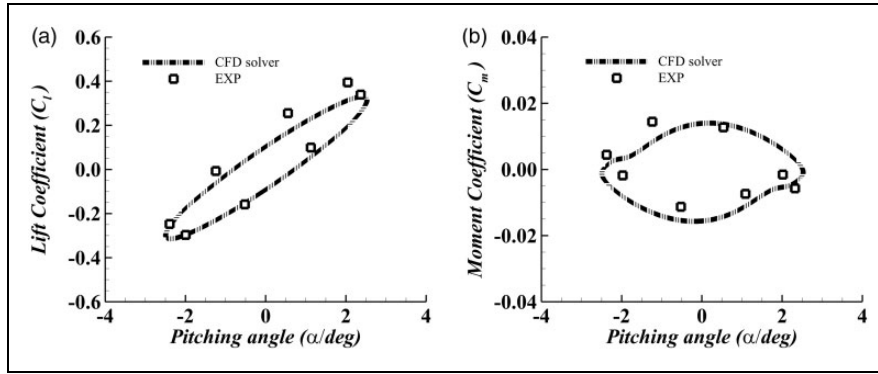


Figure 4. Comparison of the computed lift and moment coefficients with experimental data.⁵³ (a) lift coefficient; (b) moment coefficient.

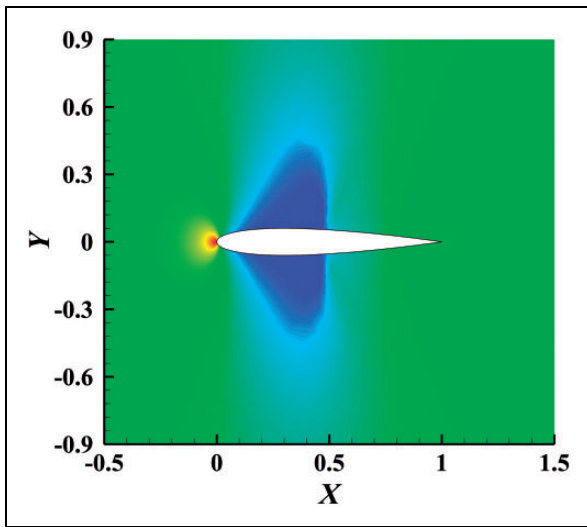


Figure 5. Steady flow of NACA0012 Airfoil at 0° AOA (Mach number 0.8).

The training case has 3000 time steps, and the delay numbers for all the models are $m=5$ and $n=4$. The errors of the predicting results are calculated as relative errors in equation (13). The relative errors reflect the global differences between the CFD results and the ROM results. The “ $C_{l\text{simulation}}$ ” means the lift coefficients of the ROMs, the “ $C_{l\text{real}}$ ” means the correct results of the CFD. In this section, the test cases are lift coefficients in transonic flow.

$$\text{relative error} = \frac{\|C_{l\text{simulation}} - C_{l\text{real}}\|_2}{\|C_{l\text{real}}\|_2} \quad (13)$$

Training case and parameter selection

Before applying the ROM to aerodynamic prediction, a training process is needed to learn the input–output relationship from data. There are many ways to design training signals, such as 3211, chirp, random signals, etc.¹⁰ Generally speaking, random signals have a wide range of frequencies and amplitudes,

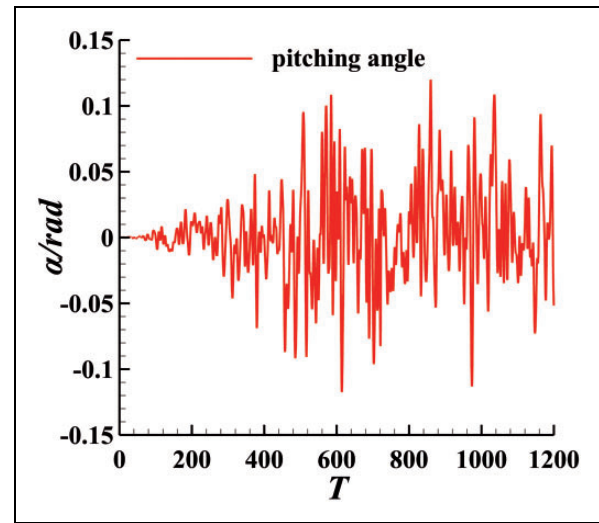


Figure 6. Pitching angle of training case (white noise).

and can cover more dynamic information with a small number of data. This signal is a common choice in ROM training.¹⁰ In this condition, we choose this training signal to guarantee the generalization capability and the accuracy of our ROMs.

As shown in Figure 6, the random training signal for the NACA0012 airfoil is designed, with a maximal amplitude of 0.12 rad (6.87°), thereby covering a large range of nonlinear aerodynamic behaviors. The reduced frequency coverage of the signal is from 0 to 0.4. Here, T represents the nondimensional time. Since the nondimensional time step DT is set to 0.4 and there are 3000 time steps, T is from 0 to 1200.

The number of neurons in the hidden layer will influence the accuracy and the generalization capability of the model. By examining the influence of the number of different centers on the accuracy of the model, the optimal number of centers can be determined. Figure 7 shows the effect of the number of the centers on the training error (relative error) and Figure 8 shows the effect on the prediction error. Note that for FSRBF neural network, this number represents the number of hidden neurons in fuzzy layer 2.

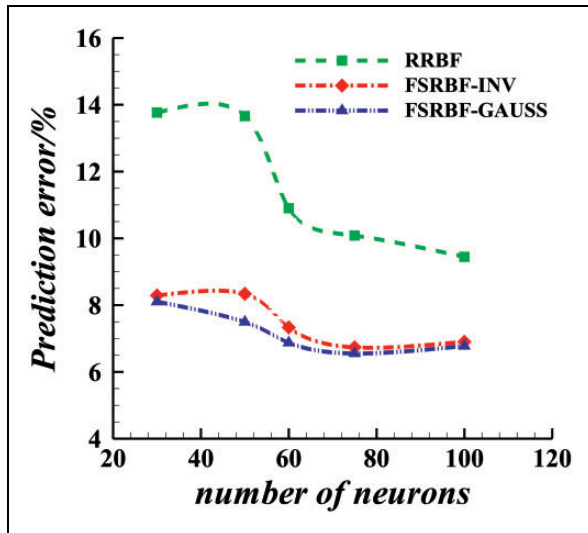


Figure 7. The relative errors of models trained at different number of centers (training error).

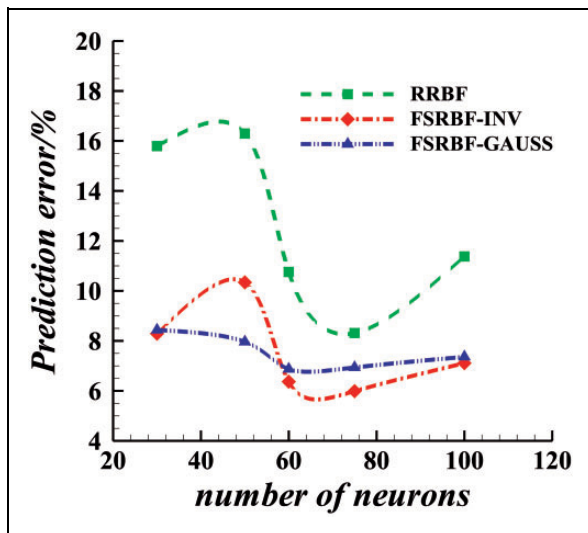


Figure 8. The relative errors of models trained at different number of centers (prediction error).

Compared with standard RRBF neural network, the FSRBF neural network model shows better accuracy at the same center number. This is due to the fact that the model becomes more flexible to different aerodynamic features. While the accuracy of RRBF neural network gradually increases with the increase in the number of neurons, excessive number of centers will inevitably lead to overfitting (the training error is small while the prediction error is very large). Therefore, in the current study, all neural networks with 75 hidden neurons are selected.

For the PSO algorithm, the number of evolution is of 40, and the population size is 20. All models use the same optimization algorithm and parameters for an objective comparison. For the RRBF neural network,

the number of parameters to be optimized is 75. For the FSRBF neural network, the number of parameters to be optimized is 675.

Test case of random motions

To check the efficacy of the FSRBF model, RRBF neural network (Gaussian function, RRBF) and FSRBF neural network (Gaussian function, FSRBF-GAUSS and inverse multiquadratic function, FSRBF-INV) are used in the time-domain prediction. Since the nondimensional time step DT is set to 0.4 and there are 1000 time steps, T is from 0 to 400. Test case are signals with the same configuration to evaluate the generalization capability at relative amplitudes of $A = 0.100, 0.050, 0.020$, and 0.005 , where the maximal pitching angles are $5.73^\circ, 2.86^\circ, 1.14^\circ$, and 0.28° , respectively. The nonlinear characteristics of aerodynamics at each maximal pitching angles is analyzed in [36].

The predicted aerodynamic loads are compared in Figure 9, the relative errors are shown in Table 1. From Figure 9(a), it can be seen that four curves are basically consistent, indicating that the scalar-based FSRBF neural network has the transonic aerodynamic response prediction capability. Although all the predicted aerodynamic forces in Figure 9(a) are accurate, with the change of the amplitude, the original RRBF model starts to deviate from the reference value. It can be seen from the table that although the accuracy of the RRBF model is the best at amplitude of 2.86° , it loses the ability to predict small-amplitude aerodynamic characteristics, which is also the limitation of the original model. For the FSRBF neural network, it realizes learning good prediction of aerodynamic characteristics at different amplitudes. These results indicate that FSRBF neural network has higher accuracy and smaller relative errors, and both models based on either the inverse multi-quadratic basis function or the Gaussian function give reasonable results. This also shows the robustness of the proposed method to different basis functions.

Test cases of harmonic motion

In the previous section, the performance in predicting the random motion is shown. However, in this section, behaviors in the harmonic motions are predicted. All the harmonic motions have the same mean pitching angle 0° and different maximum amplitudes A . Harmonic motions at two amplitudes ($A = 0.070$ rad, $A = 0.005$ rad) and two reduced frequencies ($k = 0.3271, k = 0.1635$) are used to evaluate the model. The reduced frequency k is defined as $k = \omega b / V$, where ω denotes the pitching angular velocity and V is the flow velocity.

The linear and nonlinear aerodynamic characteristics are mainly determined by the amplitude.^{36,54}

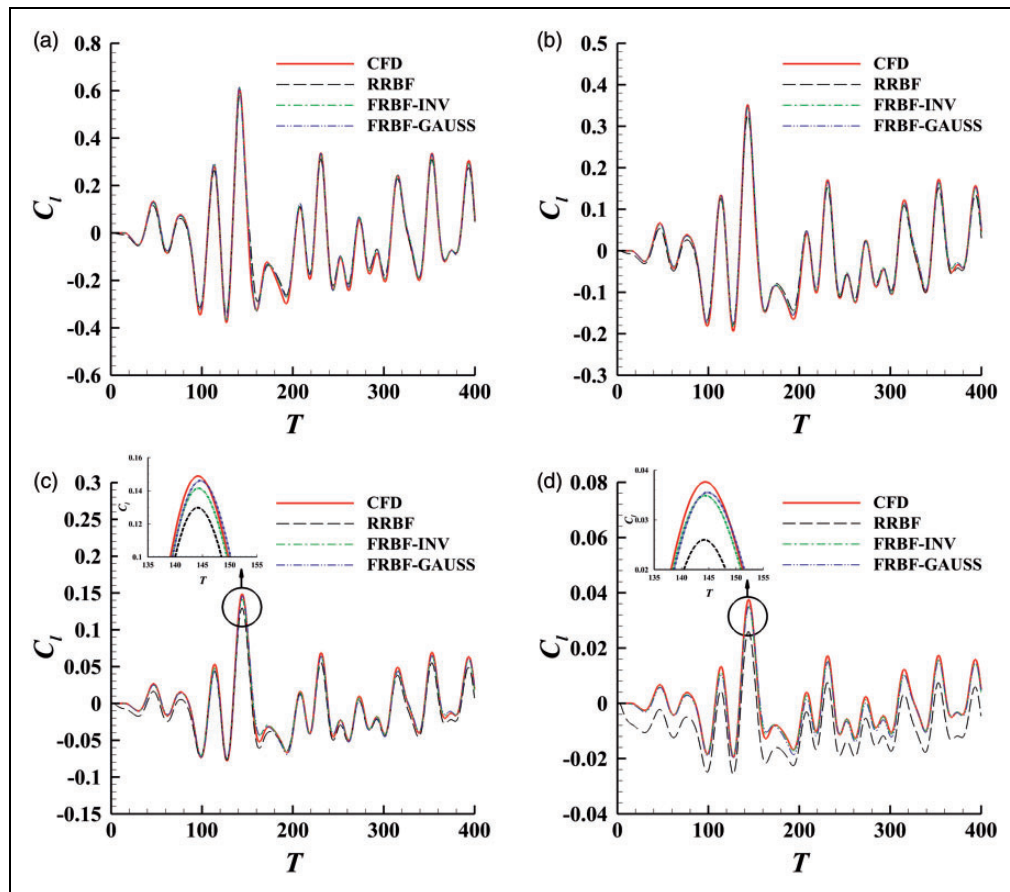


Figure 9. Results of unsteady lift coefficients (random motions): (a) $A = 0.100$ rad (5.73°); (b) $A = 0.050$ rad (2.86°); (c) $A = 0.020$ rad (1.14°); (d) $A = 0.005$ rad (0.28°).

Table 1. Relative error of lift coefficient in random motion.

| A (rad) | RRBF (%) | FSRBF-INV (%) | FSRBF-GAUSS (%) |
|---------|----------|---------------|-----------------|
| 0.100 | 15.5 | 6.8 | 7.1 |
| 0.050 | 10.8 | 7.1 | 6.8 |
| 0.020 | 24.5 | 7.9 | 9.0 |
| 0.005 | 109.4 | 9.3 | 14.1 |

Table 2. Relative error of lift coefficient in harmonic motion ($k = 0.3271$).

| A (rad) | RRBF (%) | FSRBF-INV (%) | FSRBF-GAUSS (%) |
|---------|----------|---------------|-----------------|
| 0.070 | 11.8 | 2.1 | 2.8 |
| 0.005 | 58.5 | 6.0 | 5.2 |

In this paper, the main topic is aerodynamic nonlinearity. Given a flow field at a small angle of attack and small perturbation, the flow varies slightly in a linear fashion with wing motion, which is usually defined as dynamic linear or static nonlinear aerodynamics. From previous investigation,³⁶ generally speaking, when the amplitude is lower than 1.146° , the aerodynamic characteristics are linear. When the amplitude is higher than 1.146° , the aerodynamic nonlinearity of pitching motions arises.³⁶ The method of dividing the degree of nonlinearity is consistent with the findings of Dowell and Ilgamov.⁵⁴

The aerodynamic loads of four different harmonic motions are compared. The relative errors of lift coefficient in harmonic motion are listed in Table 2 and Table 3. As can be seen from Figure 10(a) and (b), the

Table 3. Relative error of lift coefficient in harmonic motion ($k = 0.1635$).

| A (rad) | RRBF (%) | FSRBF-INV (%) | FSRBF-GAUSS (%) |
|---------|----------|---------------|-----------------|
| 0.07 | 10.5 | 4.1 | 3.9 |
| 0.005 | 41.5 | 7.4 | 7.1 |

area of the hysteresis loop of the standard RRBf neural network is significantly smaller than that of the CFD. This indicates that the standard RRBf neural network is difficult to capture the hysteresis effect at large reduced frequency $k = 0.3271$. Besides, the linear aerodynamics at low amplitudes, as shown in Figure 10(b), is also poorly captured by the standard RRBf neural network. For the FSRBF neural network model, due to the improved model structure,

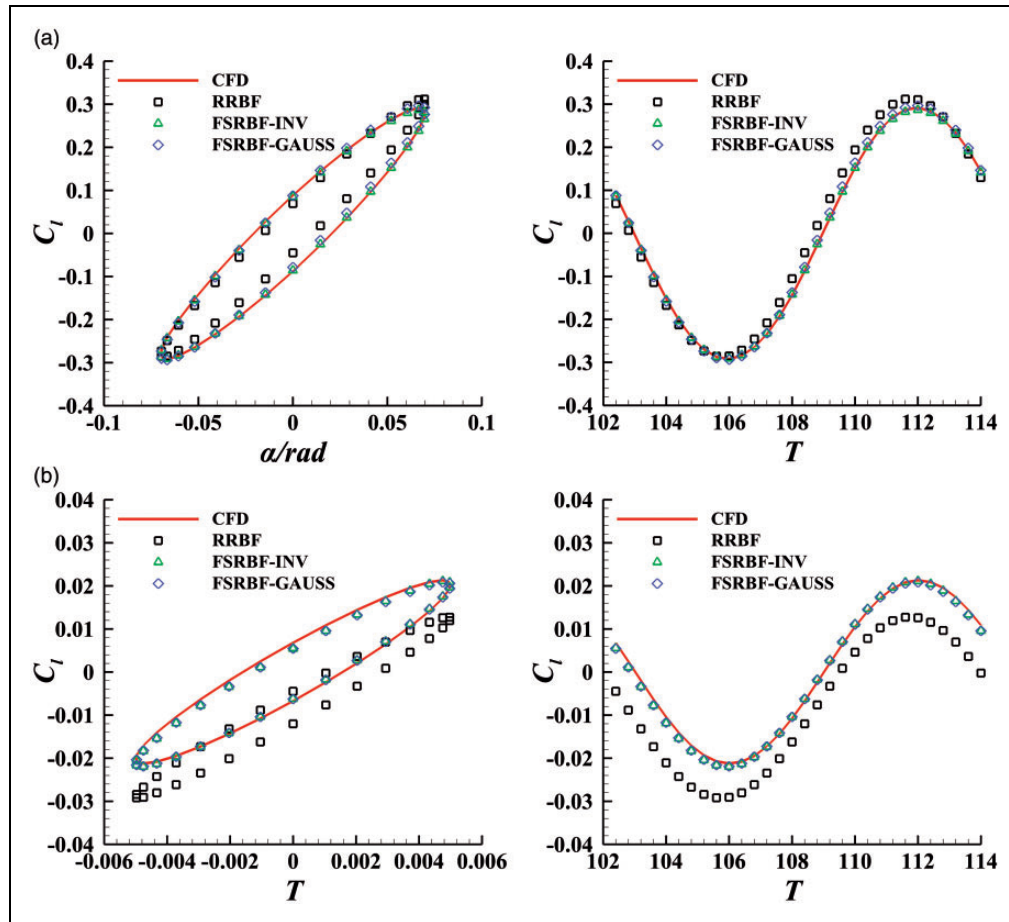


Figure 10. Result of $k = 0.3271$ case (harmonic motions): (a) $k = 0.3271$, $A = 0.070$ rad (4.01°); (b) $k = 0.3271$, $A = 0.005$ rad (0.28°).

the aerodynamics at both large and small amplitudes are depicted more accurately. Not only the area of the hysteresis loop is basically consistent, but also the prediction is accurate at each amplitude.

Observing Figure 10, at a small reduced frequency, the trend is similar. The only difference is that RRBf neural network predicts deviation when it approaches A , which affects the accuracy of the original model. Figures 10(b) and 11(b) fully show that FSRBF has good prediction on both aerodynamic linearity and nonlinearity.

In summary, the ROM method from the FSRBF neural network is significantly better than the standard RRBf neural network in the accuracy of the aerodynamic model. The proposed method can capture both linear and nonlinear aerodynamics at different amplitudes and frequencies. The scalar-based fuzzy neural network shows higher accuracy and stronger generalization capability under the same optimization conditions.

Modeling capability with different scales

Data preprocessing plays an import role in many machine learning algorithms. The normalization methods are widely used before the training process of most of the neural networks. Normalization

methods traditionally map the data to a certain range of signals, making the modeling task easier and the resulting model accurate. As a result, in real applications, multiple normalization methods can be used, which vary in accuracy and generalization capability for different problems of interest. Different normalization method in the input parameters will lead to different ROMs. In the previous research, the radian scale is used as the normalization criterion. In this section, accuracies of the models with different normalizations are compared firstly. Since different simulation cases may prefer different normalizations, a set of simulation cases will be considered. Secondly, the adaptability of the FSRBF model will also be tested. With the widths trained in fuzzy layer 1, the proposed FSRBF neural network can enhance the generalization capability greatly. Since the previous models use a vector-based basis function, the effects on different input scales are not fully reflected. In this section, we will compare the accuracy of models modeled at different scale inputs. At the reduced frequencies of 0.1635, 0.3271, the predictions of models of normalized (0–1 scale) input–output data are compared to models of radian scale and degree scale.

Figures 12 and 13 show the effect of scale on the standard RRBf neural network. When the same training samples at different input scales are

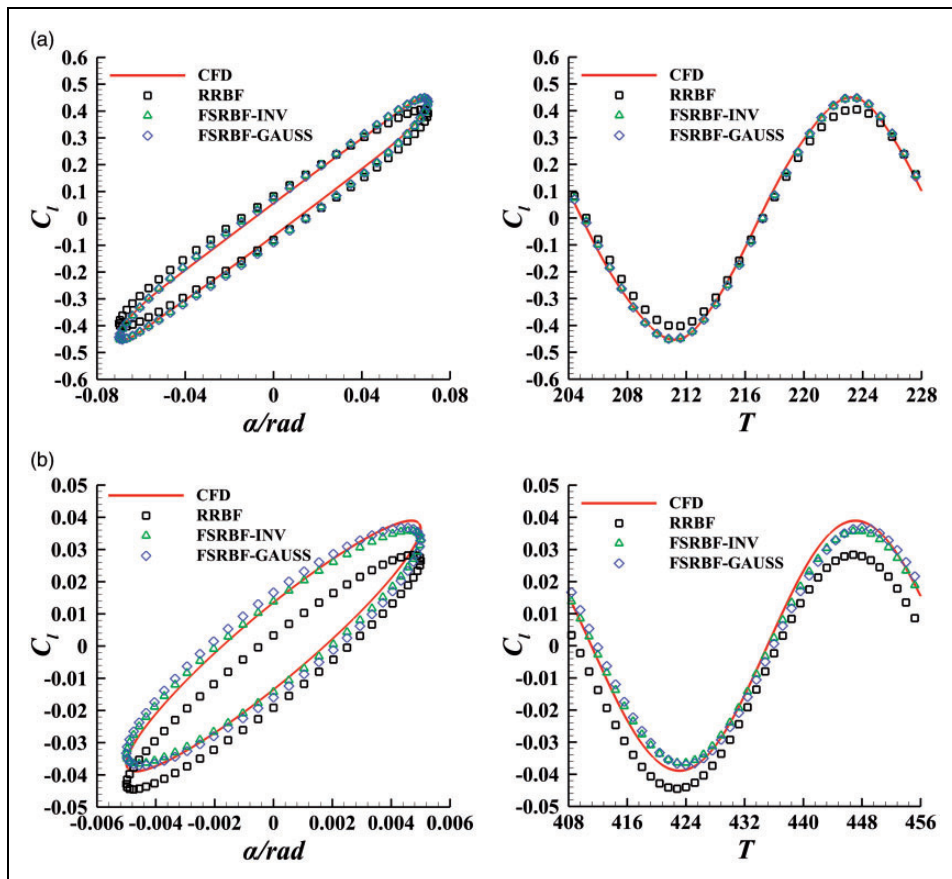


Figure 11. Result of $k = 0.1635$ case (harmonic motions): (a) $k = 0.1635$, $A = 0.070$ rad (4.01°); (b) $k = 0.1635$, $A = 0.005$ rad (0.28°).

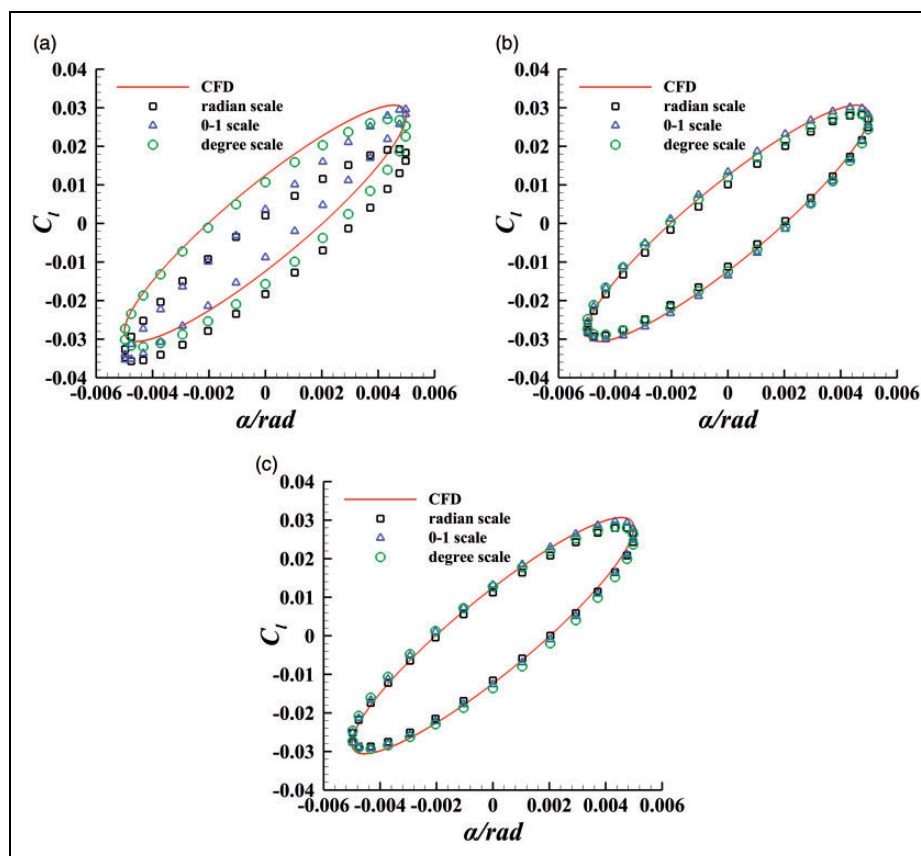


Figure 12. Different scales modeling at small amplitudes ($k = 0.1635$, $A = 0.005$ rad): (a) RRBf neural network; (b) FSRBF neural network (inverse multiquadric); (c) FSRBF neural network (Gaussian function). CFD: computational fluid dynamics.

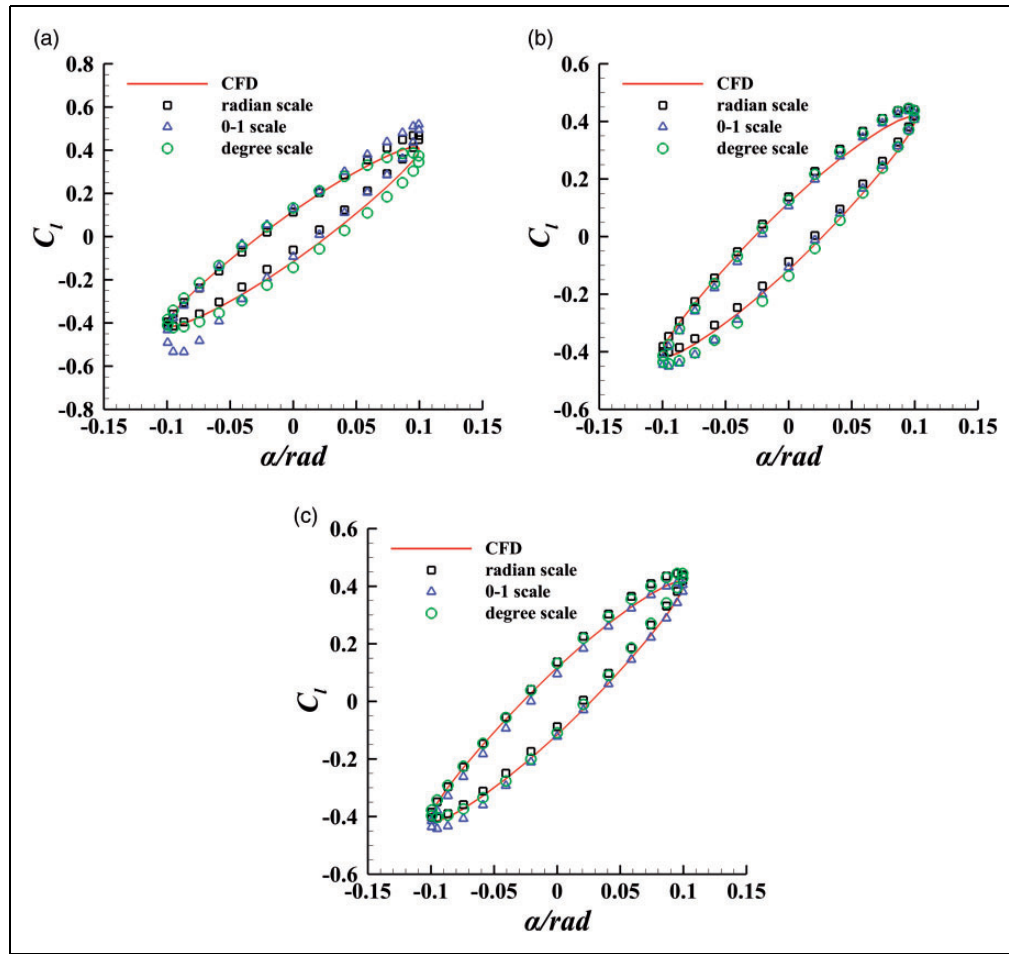


Figure 13. Different scales modeling at large amplitudes ($k=0.3271$, $A=0.100$ rad): (a) RRBF neural network; (b) FSRBF neural network (inverse multiquadratic); (c) FSRBF neural network (Gaussian function). CFD: computational fluid dynamics.

identified, the model performance in the prediction of the hysteresis loop will change dramatically. This will pose a great challenge to the modeler, since one has to determine a proper input scale. However, the fuzzy neural network with scalar basis function solves this problem, and the description of the hysteresis loop is basically the same at different scales. Furthermore, it can be seen that, although 0–1 scale is widely used in neural network modeling, it may not lead to reasonable prediction for the standard RBF neural network.

To fully evaluate the performance in modeling with multiple input scales, samples with five normalization methods (0–1 normalization, radians, degrees, minutes, and seconds) are used (1, 2, 3, 4, and 5 in the figure). Figures 14 and 15 show the influence of different input scales on all the models. For standard RBF neural network, the prediction error of the RRBF neural network will fluctuate aromatically due to the difference in scale of input parameters. However, for the FSRBF neural network, the model accuracy is improved not only at each scale, but also across a range of scales as shown in Table 4 and Table 5. In the aerodynamic prediction of small amplitude pitching motion (Figures 14(a) and 15(a)),

the relative errors hardly change with the scales, maintaining a good adaptive characteristic. With the increase of the amplitude, in Figures 14(b) and 15(b), although the prediction error of FSRBF neural network occasionally fluctuates on different scales, it still greatly improves the modeling accuracy and multiscale generalization ability. Since the use of scalar basis function, these FSRBF neural network-based models are better at adapting different input scales. This feature is very attractive for users of unsteady aerodynamic modeling and other dynamic modeling problems.

Furthermore, the time cost of the proposed approach is compared with traditional RRBF neural network in Table 6. Details of the time cost of each case are given in [10,36]. It should be mentioned that only a few typical examples are used to validate the model in this paper, but in the application of ROM, more test examples are needed. As the number of test cases increases, the computational time cost will be further reduced. Generally speaking, by using ROM for aerodynamic simulation, the computational cost of full-order simulation can be reduced by one or two orders of magnitude, which has been validated in

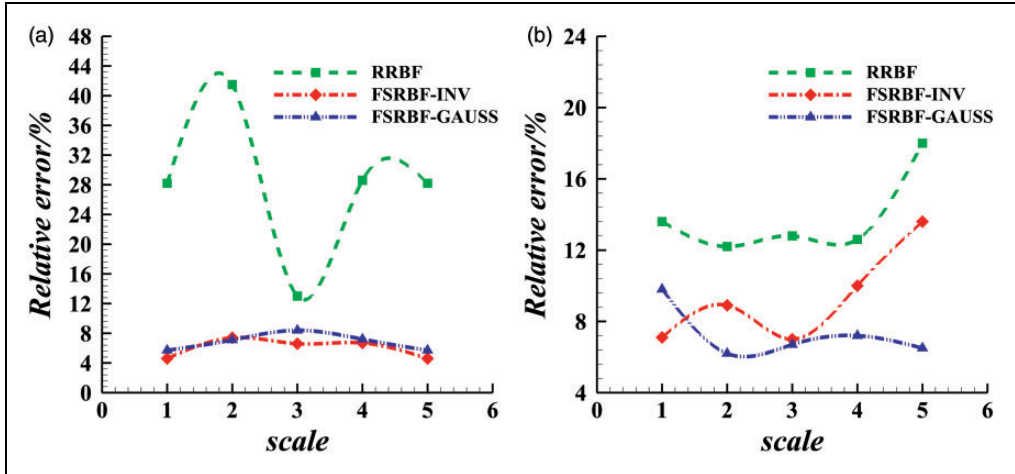


Figure 14. Relative error of lift coefficient at different input scales ($k=0.1635$): (a) $A=0.005$ rad, $k=0.1635$; (b) $A=0.1$ rad, $k=0.1635$.

Table 4. Relative error of lift coefficient in different scales ($k=0.1635$).

| Scale | RRBF (0.005/0.1 rad) (%) | FSRBF-INV (0.005/0.1 rad) (%) | FSRBF-GAUSS (0.005/0.1 rad) (%) |
|----------------|-----------------------------|----------------------------------|------------------------------------|
| 0–1 normalized | 28.2/13.6 | 4.6/7.1 | 5.7/9.8 |
| Radian | 41.5/12.2 | 7.4/8.9 | 7.1/6.2 |
| Degree | 13.0/12.8 | 6.6/7.0 | 8.4/6.7 |
| Minute | 28.6/12.6 | 6.7/10.0 | 10.1/7.2 |
| Second | 28.2/18.0 | 4.6/13.6 | 5.7/6.5 |

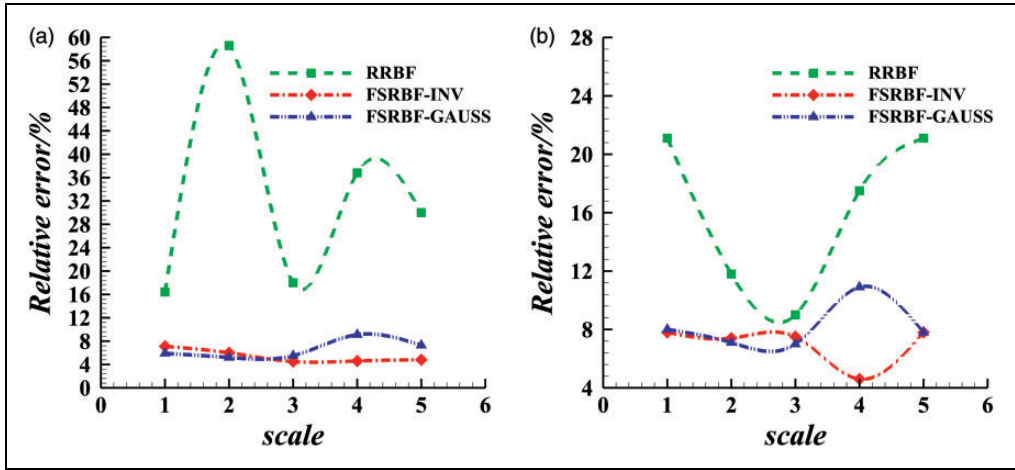


Figure 15. Relative error of lift coefficient at different input scales ($k=0.3271$): (a) $A=0.005$ rad, $k=0.3271$; (b) $A=0.1$ rad, $k=0.3271$.

Table 5. Relative error of lift coefficient in different scales ($k=0.3271$).

| Scale | RRBF (0.005/0.1 rad) (%) | FSRBF-INV (0.005/0.1 rad) (%) | FSRBF-GAUSS (0.005/0.1 rad) (%) |
|----------------|-----------------------------|----------------------------------|------------------------------------|
| 0–1 normalized | 16.4/21.1 | 7.1/7.8 | 5.9/8.0 |
| Radian | 58.6/11.8 | 6.0/7.4 | 5.2/7.1 |
| Degree | 18.0/9.0 | 4.5/7.5 | 5.5/7.0 |
| Minute | 36.8/17.5 | 4.6/4.6 | 9.1/10.9 |
| Second | 30.0/21.1 | 4.8/7.8 | 7.3/7.8 |

Table 6. Comparison of the time cost at prediction cases.

| Method | Time |
|--|---|
| CFD simulation (1 training case + 8 prediction cases) | About 110 h (30 h + 8*10 h) |
| RRBF neural network (1 training case + 8 prediction cases) | About 30.55 h (Training signal 30 h + Training time 30 min + prediction time 8*30 s) |
| FSRBF neural network (1 training case + 8 prediction cases) | About 31 h (Training signal 30 h + Training time 53 min + prediction time 8*45 s) |

aeroelastic simulation or aerodynamic prediction.^{10,31} With more parameters to optimize, the average training time of FSRBF neural network is longer than RRBF neural network. But the prediction takes about the same length of time at same cases. In summary, the new method has a higher accuracy, while it does not have a great impact on the efficiency of the reduced-order model.

Conclusion

This paper presents a fuzzy scalar neural network to construct unsteady nonlinear aerodynamic reduced-order models, in order to adapt to aerodynamic data with different scales. Through introducing the PSO algorithm and organizing the training process, the widths of the model can be optimized by training data. The Gaussian function and the inverse multi-quadratic basis functions are both selected for the FSRBF neural network. Examples show that the FSRBF neural network model can achieve accurate aerodynamic prediction from linear to nonlinear aerodynamics. Three main conclusions are drawn from the study:

1. With the use of scalar basis functions, the proposed model is adaptive to different input scales. Compared with RRBF neural networks, the performance of the proposed model is less sensitive to different input scales, thus allowing no normalization methods for data preprocessing.
2. The aerodynamic models using the FSRBF neural network exhibit a better generalization capability and higher precision in the prediction of aerodynamic coefficients.
3. Compared with deep learning neural network, the proposed FSRBF neural network is simpler in structure and clearer in physical meaning. Therefore, it is easier to be trained and to be applied to system identification problems. Future work includes the extension of this model to complex dynamic systems with multiple input types and scales, like the flight dynamics of an aircraft.


Declaration of Conflicting Interests

The author(s) declared no potential conflicts of interest with respect to the research, authorship, and/or publication of this article.

Funding

The author(s) disclosed receipt of the following financial support for the research, authorship, and/or publication of this article: This work was supported by the National Natural Science Foundation of China (No. 11572252), the National Science Fund for Excellent Young Scholars (No. 11622220) and “111” project of China (No. B17037) and ATCFD project (2015-F-016).

ORCID iD

Jiaqing Kou  <http://orcid.org/0000-0002-0965-5404>

References

1. Zhao H, Gao S, He Z, et al. Identification of nonlinear dynamic system using a novel recurrent wavelet neural network based on the pipelined architecture. *IEEE Trans Ind Electron* 2014; 61: 4171–4182.
2. Adhikari R. A neural network based linear ensemble framework for time series forecasting. *Neurocomputing* 2015; 157: 231–242.
3. Lou YF and Brunn P. An offset error compensation method for improving ANN accuracy when used for position control of precision machinery. *Neural Comput Appl* 1998; 7: 90–95.
4. Li K, Peng JX and Bai EW. A two-stage algorithm for identification of nonlinear dynamic systems. *Automatica* 2006; 42: 1189–1197.
5. Wu GD and Zhu ZW. An enhanced discriminability recurrent fuzzy neural network for temporal classification problems. *Fuzzy Sets Syst* 2014; 237: 47–62.
6. Wang X, Ma L, Wang B, et al. A hybrid optimization-based recurrent neural network for real-time data prediction. *Neurocomputing* 2013; 120: 547–559.
7. Kurtulus DF. Ability to forecast unsteady aerodynamic forces of flapping airfoils by artificial neural network. *Neural Comput Appl* 2009; 18: 359.
8. Mannarino A and Mantegazza P. Nonlinear aeroelastic reduced order modeling by recurrent neural networks. *J Fluids Struct* 2014; 48: 103–121.
9. Zhang W, Wang B, Ye Z, et al. Efficient method for limit cycle flutter analysis based on nonlinear aerodynamic reduced-order models. *AIAA J* 2012; 50: 1019–1028.
10. Kou J and Zhang W. A hybrid reduced-order framework for complex aeroelastic simulations. *Aerosp Sci Technol* 2019; 84: 880–894.
11. Zhang W and Ye Z. On unsteady aerodynamic modeling based on CFD technique and its applications on aeroelastic analysis. *Adv Mech* 2008; 38: 77–86.
12. Zhang W, Li X, Ye Z, et al. Mechanism of frequency lock-in in vortex-induced vibrations at low Reynolds numbers. *J Fluid Mech* 2015; 783: 72–102.
13. Gao C, Zhang W, Li X, et al. Mechanism of frequency lock-in in transonic buffeting flow. *Journal of Fluid Mechanics* 2017; 818: 528–561.
14. Hesse H and Palacios R. Reduced-order aeroelastic models for dynamics of maneuvering flexible aircraft. *AIAA Journal* 2014; 52(8): 1717–1732.

15. Zhang W, Chen K and Ye Z. Unsteady aerodynamic reduced-order modeling of an aeroelastic wing using arbitrary mode shapes. *Journal of Fluids and Structures* 2015; 58: 254–270.
16. Hall KC, Thomas JP and Dowell EH. Proper orthogonal decomposition technique for transonic unsteady aerodynamic flows. *AIAA Journal* 2000; 38(10): 1853–1862.
17. Willcox K and Peraire J. Balanced model reduction via the proper orthogonal decomposition. *AIAA Journal* 2002; 40(11): 2323–2330.
18. Zhang W, Ye Z and Zhang C. Aeroservoelastic analysis for transonic missile based on computational fluid dynamics. *Journal of Aircraft* 2009; 46(6): 2178–2183.
19. Li X, Liu Y, Kou J, et al. Reduced-order thrust modeling for an efficiently flapping airfoil using system identification method. *Journal of Fluids and Structures* 2017; 69: 137–153.
20. Juang JN and Pappa RS. An eigensystem realization algorithm for modal parameter identification and model reduction. *Journal of guidance, control, and dynamics* 1985; 8(5): 620–627.
21. Griffiths L M, Gaitonde A L, Jones D P, et al. Updating of aerodynamic reduced order models generated using computational fluid dynamics. Proceedings of the Institution of Mechanical Engineers, Part G: Journal of Aerospace Engineering, 2018, 232(9): 1739–1763.
22. Silva W. Identification of nonlinear aeroelastic systems based on the Volterra theory: progress and opportunities. *Nonlinear Dynamics* 2005; 39(1-2): 25–62.
23. Balajewicz M and Dowell E. Reduced-order modeling of flutter and limit-cycle oscillations using the sparse Volterra series. *Journal of Aircraft* 2012; 49(6): 1803–1812.
24. Raveh DE. Reduced-order models for nonlinear unsteady aerodynamics. *AIAA Journal* 2001; 39(8): 1417–1429.
25. Tobak M. On the use of the indicial-function concept in the analysis of unsteady motions of wings and wing-tail combinations 1954.
26. Marzocca P, Librescu L, Kim D H, et al. Development of an indicial function approach for the two-dimensional incompressible/compressible aerodynamic load modelling. Proceedings of the Institution of Mechanical Engineers, Part G: Journal of Aerospace Engineering, 2007, 221(3): 453–463.
27. Glaz B, Liu L and Friedmann PP. Reduced-order nonlinear unsteady aerodynamic modeling using a surrogate-based recurrence framework. *AIAA Journal* 2010; 48(10): 2418–2429.
28. Li X, Guo Z, Dana G, et al. Efficient reduced-order modeling of unsteady aerodynamics under light dynamic stall conditions. Proceedings of the Institution of Mechanical Engineers, Part G: Journal of Aerospace Engineering, 2018: 0954410018773628.
29. Da Ronch A, Ghoreyshy M and Badcock KJ. On the generation of flight dynamics aerodynamic tables by computational fluid dynamics. *Progress in Aerospace Sciences* 2011; 47(8): 597–620.
30. Wang Bobin, Zhang Weiwei and Ye Zhengyin. Unsteady nonlinear aerodynamics identification based on neural network model. *Acta Aeronautica et Astronautica Sinica* 31.7 2010; 1379–1388. (in Chinese).
31. Kou J, Zhang W and Yin M. Novel Wiener models with a time-delayed nonlinear block and their identification. *Nonlinear Dynamics* 2016; 85(4): 2389–2404.
32. Huang R, Hu H and Zhao Y. Nonlinear reduced-order modeling for multiple-input/multiple-output aerodynamic systems. *AIAA Journal* 2014; 52(6): 1219–1231.
33. Ghoreyshy M, Cummings RM, Ronch AD, et al. Transonic aerodynamic load modeling of X-31 aircraft pitching motions. *AIAA journal* 2013; 51(10): 2447–2464.
34. Winter M and Breitsamter C. Neurofuzzy-model-based unsteady aerodynamic computations across varying free-stream conditions. *AIAA Journal* 2016; 2705–2720.
35. Dey P, Sarkar A and Das AK. Development of GEP and ANN model to predict the unsteady forced convection over a cylinder. *Neural Computing and Applications* 2016; 27(8): 2537–2549.
36. Kou J and Zhang W. An approach to enhance the generalization capability of nonlinear aerodynamic reduced-order models. *Aerospace Science and Technology* 2016; 49: 197–208.
37. Billings SA, Wei HL and Balikhin MA. Generalized multiscale radial basis function networks. *Neural Networks* 2007; 20(10): 1081–1094.
38. Zhang W, Guo X, Wang C, et al. A POD-based center selection for RBF neural network in time series prediction problems//International Conference on Adaptive and Natural Computing Algorithms. Springer, Berlin, Heidelberg, 2007: 189–198.
39. Fernández-Navarro F, Hervás-Martínez C, Sánchez-Monedero J, et al. MELM-GRBF: a modified version of the extreme learning machine for generalized radial basis function neural networks. *Neurocomputing* 2011; 74(16): 2502–2510.
40. Kou J and Zhang W. Multi-kernel neural networks for nonlinear unsteady aerodynamic reduced-order modeling. *Aerospace Science and Technology* 2017; 67: 309–326.
41. Winter M and Breitsamter C. Nonlinear identification via connected neural networks for unsteady aerodynamic analysis. *Aerospace Science and Technology* 2018; 77:802–818.
42. Han HG, Zhang S and Qiao JF. An adaptive growing and pruning algorithm for designing recurrent neural network. *Neurocomputing* 2017; 242: 51–62.
43. Chen S, Billings SA, Cowan CFN, et al. Non-linear systems identification using radial basis functions. *International Journal of Systems Science* 1990; 21(12): 2513–2539.
44. Jang JSR and Sun CT. Functional equivalence between radial basis function networks and fuzzy inference systems. *IEEE Transactions on Neural Networks* 1993; 4(1): 156–159.
45. Boely N, Botez R M, Kouba G. Identification of a nonlinear F/A-18 model by the use of fuzzy logic and neural network methods. Proceedings of the Institution of Mechanical Engineers, Part G: Journal of Aerospace Engineering, 2011, 225(5): 559–574.
46. Cho KB and Wang BH. Radial basis function based adaptive fuzzy systems and their applications to system identification and prediction. *Fuzzy Sets and Systems* 1996; 83(3): 325–339.
47. El-Sousy FFM. Adaptive hybrid control system using a recurrent RBFN-based self-evolving fuzzy-neural-

- network for PMSM servo drives. *Applied Soft Computing* 2014; 21: 509–532.
48. Eberhart R, Kennedy J. A new optimizer using particle swarm theory//Micro Machine and Human Science, 1995. MHS'95., Proceedings of the Sixth International Symposium on. IEEE, 1995: 39-43.
 49. Spalart PRA and Allmaras S. A one-equation turbulence model for aerodynamic flows//30th aerospace sciences meeting and exhibit1992; 439.
 50. De Boer A, Van der Schoot MS and Bijl H. Mesh deformation based on radial basis function interpolation. *Computers & Structures* 2007; 85(11-14): 784–795.
 51. Jiang Y. Numerical solution of Navier–Stokes equations on generalized mesh and its applications. NWPU, Xi'an, China (Ph. D. thesis), 2013.
 52. Zhu L, Zhang W, Kou J, et al. Machine learning methods for turbulence modeling in subsonic flows around airfoils. *Physics of Fluids* 2019; 31(1): 015105.
 53. Landon R H. NACA 0012 oscillatory and transient pitching[R]. AIRCRAFT RESEARCH ASSOCIATION LTD BEDFORD (UNITED KINGDOM), 2000.
 54. Dowell EH and Ilgamov M. *Studies in nonlinear aeroelasticity*. Springer Science & Business Media, 2012.